Advances in Water Resources 60 (2013) 121–134

Contents lists available at ScienceDirect

Advances in Water Resources

journal homepage: www.elsevier.com/locate/advwatres

Bias adjustment of satellite rainfall data through stochastic modeling: Methods development and application to Nepal

Marc F. Müller *, Sally E. Thompson

Department of Civil and Environmental Engineering, University of California, Davis Hall, Berkeley, CA, USA

ARTICLE INFO

Article history:
Received 8 May 2013
Received in revised form 27 July 2013
Accepted 1 August 2013
Available online 11 August 2013

Keywords:
Bias correction
Remote sensing
Stochastic model
Areal precipitation
Rainfall interpolation
Himalayas

ABSTRACT

Estimating precipitation over large spatial areas remains a challenging problem for hydrologists. Sparse ground-based gauge networks do not provide a robust basis for interpolation, and the reliability of remote sensing products, although improving, is still imperfect. Current techniques to estimate precipitation rely on combining these different kinds of measurements to correct the bias in the satellite observations. We propose a novel procedure that, unlike existing techniques, (i) allows correcting the possibly confounding effects of different sources of errors in satellite estimates, (ii) explicitly accounts for the spatial heterogeneity of the biases and (iii) allows the use of non overlapping historical observations. The proposed method spatially aggregates and interpolates gauge data at the satellite grid resolution by focusing on parameters that describe the frequency and intensity of the rainfall observed at the gauges. The resulting gridded parameters can then be used to adjust the probability density function of satellite rainfall observations at each grid cell, accounting for spatial heterogeneity. Unlike alternate methods, we explicitly adjust biases on rainfall *frequency* in addition to its intensity. Adjusted rainfall distributions can then readily be applied as input in stochastic rainfall generators or frequency domain hydrological models. Finally, we also provide a procedure to use them to correct remotely sensed rainfall time series.

We apply the method to adjust the distributions of daily rainfall observed by the TRMM satellite in Nepal, which exemplifies the challenges associated with a sparse gauge network and large biases due to complex topography. In a cross-validation analysis on daily rainfall from TRMM 3B42 v6, we find that using a small subset of the available gauges, the proposed method outperforms local rainfall estimations using the complete network of available gauges to directly interpolate local rainfall or correct TRMM by adjusting monthly means. We conclude that the proposed frequency-domain bias correction approach is robust and reliable compared to other bias correction approaches.

1. Introduction

Spatially explicit rainfall estimates are crucial for hydrologic predictions, but due to challenges in observing rainfall at watershed scales, rainfall estimates remain a major source of uncertainty for hydrologic models [1]. In many parts of the world, ground-based rain-gauge networks are irregular and locally sparse [2], and may be biased with respect to the sources of environmental variability (see Fig. 1 for an example). Such networks do not provide a robust basis for inferring the spatial pattern of rainfall fields. An alternative and explicitly spatial rainfall product is provided by satellite observations of precipitation. Unfortunately, satellite observations of rainfall have widely acknowledged limitations, including sensitivity to precipitation type [3], underestimation of orographic rainfall [4], a tendency to miss snowfall [5], inability to capture short rainfall events [6] and systematic biases in mountainous areas [5,7–9]. Using ground-based data to correct biases in satellite data provides one method to address these limitations. For example, the satellite observations in the NASA Tropical Rainfall Measuring Mission (TRMM) 3B42 dataset are adjusted using monthly-averaged ground observations provided by local monitoring agencies to the Global Precipitation Climatology Centre (GPCC) [3]. However, the efficiency of the adjustment is limited by the scarcity of available gauges and typically requires careful regional evaluation against local precipitation measurements.

The correction applied by NASA on TRMM is a standard bias adjustment procedure for satellite rainfall observations, based on correcting rainfall time series – in this case by regression analysis applied to cumulative rainfall totals [7,10,11]. Other standard procedures adjust quantiles of the daily rainfall to match those observed at gauges [12]. These approaches suffer from several drawbacks:

* Corresponding author.
E-mail addresses: marc.muller@berkeley.edu (M.F. Müller), sally.thompson@berkeley.edu (S.E. Thompson).

0309-1708/$ - see front matter © 2013 Elsevier Ltd. All rights reserved.
http://dx.doi.org/10.1016/j.advwatres.2013.08.004

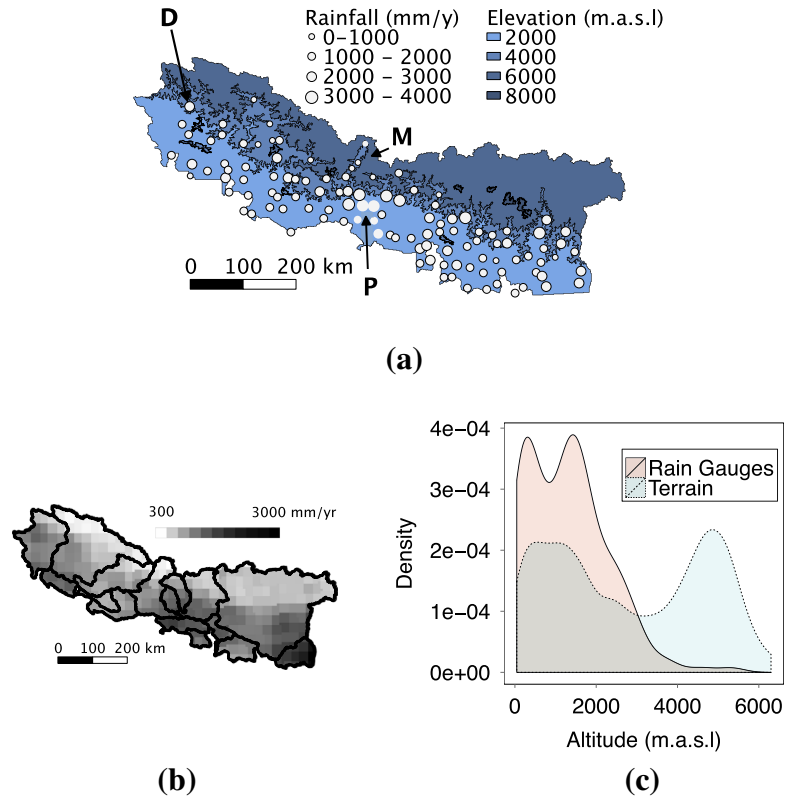

Fig. 1. Study region and available data. (a) Location of the available gauges and mean annual rainfall. The figure shows vast zones in the North that are not covered by the gauge network. The difference in annual rainfall between Pokhara (P) and Mustang (M), two proximate regions separated by the Annapurna range, illustrates the importance of rain shadow effects. The example of time series correction described in Section 3.2.6 focuses on the rainfall gauge at Darchula (D) in western Nepal. (b) Yearly rainfall in 2010 measured by TRMM 3B43 v6 (monthly precipitation) and aggregated annually, showing decreasing trends towards the east and north. (c) Kernel density estimates of the altitude distributions of the area and of the rain gauges. The figure shows that the altitude distribution of the area is bimodal with modes at 1000 masl and 5000 masl. This distribution is not matched by the gauges, which are preferentially located below 3000 masl.

1. Biases in TRMM observations of rainfall timeseries are influenced by errors in both rainfall frequency and rainfall intensity, which may have opposite signs [13]. Adjusting satellite precipitation totals or PDFs will thus correct errors in the magnitude of rainfall, but not in its temporal structure, although both factors are important for hydrological predictions [14,15].
2. Although some recent studies account for the observed spatial heterogeneity in biases, and in doing so significantly improved the corrected dataset [10,11], approaches based on preserving regional rainfall totals often do not account for spatial patterns in bias or focus on single precipitation stations. One of the factors that makes spatially-explicit corrections challenging is the upscaling of point observations from gauges to areal rainfall at the resolution of the satellite grid.
3. Finally, correction of monthly time series on a pixel by pixel basis is numerically intensive, and cannot take advantage of historical rainfall datasets which, although not overlapping with contemporary observations, may still contain useful information about spatial patterns in rainfall.

We therefore propose an alternative strategy for bias adjustment of satellite rainfall data using ground-based gauge observations. Instead of adjusting daily rainfall to match the mean monthly precipitation, we perform the bias adjustment on a set of (pseudo) stationary stochastic parameters that describe the rainfall process in terms of frequency, intensity, and the autocorrelation of wet and dry periods [16–18]. This approach addresses the key limitations of time series based bias adjustment:

1. It is a direct response to the observation of different directionality in TRMM-gauge bias arising due to different and independent features of the rainfall time series [13]. This observation implies that separating the bias adjustment for rainfall occurrence and intensity might improve the robustness of the resulting rainfall estimates.
2. It allows different features of rainfall to be independently interpolated accounting for spatial heterogeneity and, unlike existing studies, also accounting for potential differences in spatial heterogeneities between stochastic rainfall features.
3. Being in the frequency domain, the bias adjustment can be operated using non overlapping observed time series provided stationarity conditions are satisfied.

A key contribution of the proposed procedure lies in its ability to spatially aggregate and interpolate the stochastic rainfall descriptors at the grid resolution. This provides a ground truth estimate of the daily rainfall distribution at each pixel that can be used to correct satellite rainfall distributions, with two potential applications. Firstly, grid-scale rainfall cumulative probability densities are valuable for correcting rainfall timeseries magnitudes via quantile mapping [12]. Our proposed method explores the upscaling of gauge-derived rainfall PDFs and their spatial interpolation, allowing corrections to the rainfall CDF to be applied in a spatially explicit fashion. Moreover, the procedure upscales and interpolates information about the autocorrelation of rainfall, allowing the bias adjustment procedure to correct the temporal structure of satellite rainfall observations as well as the magnitudes. Since the temporal structure of rainfall is an important driver of hydrological re-

sponses in the vadose zone [14] and in the flow regime [15], incorporating this information into satellite bias correction is a useful advance. The stochastic parameters may be directly utilized in stochastic description of the resulting streamflow [15]; used to generate ensembles of synthetic time series data using stochastic weather generation models [19,20], or incorporated into time-series correction approaches (as outlined in Section 2.5).

The proposed approaches are illustrated here using Nepal as a case study. Nepal provides an excellent opportunity to test the new bias correction procedure because two satellite rainfall products are available that incorporate very different bias-adjustment techniques: TRMMv6 and TRMMv7. The major distinction between the two datasets for terrestrial rainfall estimates lies in the rain gauge datasets used for monthly bias adjustment [21]. In Nepal the number of considered gauges increases from 11 (GPCC monitoring dataset v2) to 280 gauges (GPCC full analysis dataset v6). Thus, TRMMv6 in Nepal represents a satellite rainfall data product with minimal ground-based correction, while TRMM v7 represents satellite data corrected using conventional time series adjustment. In this study, we therefore develop a bias adjustment technique, apply it to TRMM v6 and compare the results against the performance of TRMM v7 as a benchmark.

We first describe a stochastic rainfall model (Section 2.1) and its use to adjust satellite rainfall observation biases through space. Spatial adjustment of stochastic parameters is not straightforward because of their nonlinear relationships to the moments and time-structure of the rainfall distribution. To estimate bias, the stochastic model parameters obtained from point-scale rainfall measurements at gauges are spatially aggregated to the scale of a satellite observation pixel (Section 2.2). The stochastic model parameters estimated at the pixel scale are then spatially interpolated to provide estimates at the satellite pixels devoid of gauges (Section 2.3). Section 2.4 summarizes the method to correct the bias of gridded, remotely sensed daily rainfall observations in the frequency domain using multi-site gauge observations – the main contribution of this paper. Using bias adjusted frequency domain information, rainfall time series can then easily be adjusted through quantile mapping (Section 2.5). An illustrative example of time series correction is given in Section 3.2.6. The remainder of the paper focuses on assessing the performance of the frequency domain bias correction method, which underpins both the stochastic and time-series adjustments. The sensitivity of the method to common sources of uncertainties is first assessed in a Monte Carlo analysis (Section 3.1), and its ability to adjust the frequency, mean intensity and variance of actual remote sensing rainfall data is assessed in a cross validation analysis using Nepalese rainfall for various densities of gauge networks (Section 3.2). The main results and their implications are discussed in Section 4 and Section 5 concludes. Acronyms are listed in Table 1.

Table 1
Acronyms, variables and subscripts.

SMP	Stochastic model parameter
MAE	Mean absolute error
X	Daily precipitation
P	Probability of daily precipitation occurrence
N_p	Number of gauges in the considered pixel
N_g	Number of gauges to interpolate from
N_{MC}	Number of Monte Carlo rounds
N_{CV}	Number of cross validation rounds
a_i	Fraction of pixel occupied by the Thiessen polygon of gauge i
$v_i^{(\text{param})}$	Interpolation weight associated to gauge i and parameter param
$C(d)$	Correction factor on variance for areal rainfall on in a pixel of diagonal d
i	Subscript for gauges (point rainfall)
pt	Subscript for pixels aggregated from gauges (point rainfall)
pix	Subscript for pixels aggregated from gauges (areal rainfall)
TRMM	Subscript for TRMM pixels
wet	Subscript for rainy days
j	Subscript for Monte Carlo or cross validation rounds

2. Theory

2.1. Stochastic model

We use a two-step stochastic weather generator to represent the statistical properties of the rainfall time series. We firstly disaggregate the time series into two independent seasons [16] the dry season and the monsoon. We identify the seasons by the calendar days corresponding to the average start date (RnStr) and end date (RnStp) of the monsoon. Next, we describe the rainfall for each season in terms of two stochastic processes: the daily occurrence, and daily intensity of rainfall. We use a first-order Markov chain model to represent rainfall occurrence [17,18]. This model is governed by two parameters P_{01} and P_{11}, which characterize the probability of a rainy day, conditional on the previous day being dry (P_{01}) or rainy (P_{11}). We use a gamma distribution with shape parameter GS and rate parameter GR to describe the probability distribution of daily rainfall depths on those days when rain occurred. This representation of rainfall requires a total of 10 *stochastic model parameters* (SMPs) listed in Table 2. These model parameters are directly related to a range of relevant metrics that describe rainfall distribution and can thus be used to evaluate the bias adjustment method. These metrics are derived in Appendix A and include the length of wet and dry spells, the number of rainy days per year, the unconditional variance on daily rainfall and the average annual rainfall.

2.2. Areal aggregation of stochastic model parameters

While gauges monitor precipitation at particular points, satellites observe an areally averaged value of rainfall over many square kilometers. Correcting remote sensing precipitation observations therefore requires spatially aggregating point-scale precipitation parameters to the level of the satellite resolution. We perform this aggregation analytically, rather than directly from the time series because (i) it is more computationally efficient and (ii) it allows us to use data provided by on (stationary) rainfall gauges that do not overlap in time with the TRMM observation window. We outline the applicability of the methods to the case study with TRMM in Nepal below, including an evaluation of the stationarity of ground-based rainfall measurements in terms of the 10 SMPs.

2.2.1. Seasonal parameters

We assume that the starting day of the rainy and dry seasons at the pixel level can be approximated by the weighted average of the corresponding values across the N_p gauges in the pixel,

Table 2
Stochastic model parameters (SMP).

$P_{01}^{(w)}$	Probability of a dry day being followed by a wet day in the wet season
$P_{01}^{(d)}$	Probability of a dry day being followed by wet day in the dry season
$P_{11}^{(w)}$	Probability of a wet day being followed by wet day in the wet season
$P_{11}^{(d)}$	Probability of a dry day being followed by wet day in the wet season
$\text{GS}^{(w)}$	Gamma shape parameter for daily rainfall depth in the wet season
$\text{GS}^{(d)}$	Gamma shape parameter for daily rainfall depth in the dry season
$\text{GR}^{(w)}$	Gamma rate parameter for daily rainfall depth in the wet season
$\text{GR}^{(d)}$	Gamma rate parameter for daily rainfall depth in the dry season
RnStr	Average calendar day when monsoon starts
RnStp	Average calendar day when monsoon ends

$$\mathrm{Str}_{\mathrm{pix}} = \sum_{i=1}^{N_p} a_i \mathrm{Str}_i \quad \mathrm{Str} \in \{\mathrm{RnStr}, \mathrm{RnStp}\} \tag{1}$$

where a_i is the proportion of the pixel's area covered by a Thiessen polygon centered on gauge i.

2.2.2. Occurrence parameters

A pixel should be classified as 'rainy' on a given day if rain occurs at *any* of its gauges during that day. Thus the probability of rain at the level of a pixel is not a simple average of the occurrence probabilities at the gauges within the pixel, but is modified by the correlation between the gauges. If the correlation length-scale of rainfall exceeds the pixel size, then it is reasonable to assume that the correlation between the rain occurrence probabilities P_i at the different gauges is positive and maximal. That is, if the gauge that is most likely to receive rainfall is dry, the pixel is also dry. Using this assumption, the probability of rainfall in a pixel is well approximated by the maximum occurrence probability across the N_p gauges within that pixel, as:

$$P_{\mathrm{pix}} \approx \max P_i \tag{2}$$

A similar assumption about the ratio of wet-to-wet transitions $P_i \cdot P_{11,i}$ leads to the following estimate for the pixel-level transition probability:

$$P_{11,\mathrm{pix}} \approx \max\left\{\frac{\max(P_i \cdot P_{11,i})}{P_{\mathrm{pix}}}; 1 - \frac{\sum_{i=1}^{N} P_i \cdot (1 - P_{11,i})}{P_{\mathrm{pix}}}\right\} \tag{3}$$

where the transition probability P_{11} at the satellite pixel level can be approximated by its lower bound. This bound is given by the higher of (i) the maximal value of wet-to-wet ratio ($P \cdot P_{11}$) and (ii) the sum of wet-to-dry transition ratios ($P \cdot P_{10}$) within that pixel. The full derivation of Eqs. (2) and (3) is presented in Appendix B. Our case study in Nepal is characterized by a maximum density of 5 gauges per pixel and spatial autocorrelation ranges of approximately 3 (dry season) to 4 (wet season) times the pixel size of 27.7 km (Table 4), meeting the assumptions used in the derivation of Eqs. (2) and (3). We tested the performance of the aggregation equations via a Monte Carlo analysis. We found that using Eqs. (2) and (3) generated less than 2% error in both metrics (P_i and $P_i \cdot P_{11,i}$). This error declined with an increase in the correlation length scale, but increased with increasing numbers of gauges per pixel.

2.2.3. Intensity parameters

To aggregate rainfall intensity we preserve the weighted average of the first two moments of the distributions measured at each gauge, using the Thiessen polygon area ratios a_i as weights. Doing so based on the SMPs that describe the rainfall intensity (GS and GR) poses three challenges. Firstly, the SMPs are non linearly related to the moments of the gamma distribution:

$$\mathrm{E}[X \mid \mathrm{wet}] = \mathrm{GS}/\mathrm{GR} \tag{4}$$

$$\mathrm{Var}(X \mid \mathrm{wet}) = \mathrm{GS}/\mathrm{GR}^2 \tag{5}$$

Thus, aggregating the weighted sum of the distribution's parameters is not equivalent to aggregating the distribution's moments. Secondly, the parameters represent the distribution of rainfall intensity *conditional* on rainfall occurrence, so the probability P of rainfall occurrence must be incorporated into the aggregation. Finally, the variance of areal rainfall is affected by spatial autocorrelation. A full derivation of the upscaling relationship for the rainfall intensity properties, accounting for these three challenges, is provided in Appendix C. The methodology used consists of (i) conditioning for rainfall occurrence and the location of individual gauges, (ii) applying the laws of iterated expectation and total variance to compute the mean and variance of rainfall intensity at the pixel scale (Eqs. (6) and (7)) and (iii) correcting the variance of areal rainfall to account for the transition from point to areal probabilities [22]. We assume the same functional form of the PDF applies to pixels and all gauges, meaning that the pixel-scale rainfall intensity is a gamma distribution and that its parameters GS and GR are directly related to its mean and variance as in Eqs. (4) and (5). With these assumptions, we obtain the expectation and variance of the pixel-level areal rainfall as:

$$\mathrm{E}[X_{\mathrm{pix}} \mid \mathrm{wet}] = \frac{1}{P_{\mathrm{pix}}} \cdot \sum_{i=1}^{N} a_i P_i \mathrm{E}[X_i \mid \mathrm{wet}] \tag{6}$$

$$\begin{aligned}\mathrm{Var}(X_{\mathrm{pix}} \mid \mathrm{wet}) &= \frac{C(d)}{P_{\mathrm{pix}}}\left[\sum_{i=1}^{N} a_i P_i \Big(\mathrm{Var}(X_i \mid \mathrm{wet}) + P_i \mathrm{E}[X_i \mid \mathrm{wet}]^2 - P_i \mathrm{E}[X_i \mid \mathrm{wet}]\Big)\right] \\ &+ C(d) P_{\mathrm{pix}}\left[\mathrm{E}[X_{\mathrm{pix}} \mid \mathrm{wet}] - \mathrm{E}[X_{\mathrm{pix}} \mid \mathrm{wet}]^2\right]\end{aligned} \tag{7}$$

where P_i is the probability of rainfall occurrence at the gauge level, and P_{pix} is the probability of rainfall occurrence at the pixel level (from Eq. (2)). $C(d)$ is an attenuation factor applied to the variance of areal rainfall based on the derivation of Rodriguez-Iturbe and Mejía [22]:

$$C(d) = \int^{\sqrt{2}d} r(v) f(v) \mathrm{d}v \leqslant 1,$$

where $r(v)$ is the spatial correlation function of rainfall intensity and $f(v)$ is the distribution of distances between two points chosen at random in the pixel. Point-scale rainfall typically over-estimates the variance of areal rainfall, so $C(d) < 1$. $C(d)$ increases with pixel size d and decreases with the spatial autocorrelation range, both of which are typically spatially homogenous. In Nepal we estimated $C(27.7\ \mathrm{km})$ as 0.75 in the monsoon and 0.86 in the dry season, using a correlogram estimated from the spatial distribution of rainfall intensity at gauges over 2,000 randomly selected days.

2.3. Spatial interpolation of stochastic model parameters

A typical spatial interpolation methodology would approximate daily rainfall $\tilde{X}$ at unmonitored locations as linear combinations of X_i the rainfall measured at surrounding locations i on the same day, weighted by v_i^X, a normalized similarity metric based on relative position (e.g. inverse weighted distance) or the spatial correlation function of X (e.g. kriging):

$$\tilde{X} = \sum_{i=1}^{N_g} v_i^{(X)} X_i \tag{8}$$

Interpolation of the probabilistic descriptors of the rainfall, however, cannot be undertaken by directly interpolating the SMP's because neither the moments of the gamma distribution of conditional rainfall intensity nor the moments of the binomial distribution of daily rainfall occurrence are linear combinations of the SMPs. Thus, we interpolate the moments of the distributions, expressed as functions of the SMPs. We assume that interpolation must preserve seasonal transition dates (RnStr and RnStp), the daily occurrence probability of rainfall (P) and the ratio of wet-to-wet transitions ($P \cdot P_{11}$). This allows us to express the interpolated rainfall metrics as linear combinations of their respective values at the N_g observed locations, which are directly related to the observed SMPs:

$$\widetilde{\mathrm{Str}} = \sum_{i=1}^{N_g} v_i^{(\mathrm{Str})} \mathrm{Str}_i \quad \mathrm{Str} \in \{\mathrm{RnStr}, \mathrm{RnStp}\} \tag{9}$$

$$\tilde{P} = \sum_{i=1}^{N_g} v_i^{(P)} P_i = \sum_{i=1}^{N_g} v_i^{(P)} \frac{P_{01,i}}{1 + P_{01,i} - P_{11,i}} \tag{10}$$

$$\widetilde{P \cdot P_{11}} = \sum_{i=1}^{N_g} v_i^{(P \cdot P_{11})} P_i \cdot P_{11,i} = \sum_{i=1}^{N_g} v_i^{(P \cdot P_{11})} \frac{P_{11,i} P_{01,i}}{1 + P_{01,i} - P_{11,i}} \tag{11}$$

Using similar reasoning to that in Section 2.2, but replacing area weights a_i with interpolation weights $v_i^{(E)}$, we compute the interpolated moments of the distribution of conditional rainfall intensity. Here we use weights $v_i^{(E)}$ generated from kriging of the expected rainfall $E[X_i]$ for the interpolation of both the mean and variance of the rainfall PDF. Either ordinary kriging or univerval kriging can be used [23,24]. For this interpolation, we do not use the attenuation factor $C(d)$ as there is no point to area transformation. From Eqs. (6) and (7) we obtain the expectation and variance of the rainfall at the ungauged location:

$$E\left[\tilde{X} \mid \text{wet}\right] = \frac{1}{\tilde{P}} \cdot \sum_{i=1}^{N_g} v_i^{(E)} P_i E[X_i \mid \text{wet}] \tag{12}$$

$$\begin{aligned} \text{Var}\left(\tilde{X} \mid \text{wet}\right) = & \frac{1}{\tilde{P}} \left[\sum_{i=1}^{N_g} v_i^{(E)} P_i \left(\text{Var}(X_i \mid \text{wet}) + P_i E[X_i \mid \text{wet}]^2 - P_i E[X_i \mid \text{wet}] \right) \right] \\ & + \tilde{P} \left[E\left[\tilde{X} \mid \text{wet}\right] - E\left[\tilde{X} \mid \text{wet}\right]^2 \right] \end{aligned} \tag{13}$$

where P_i is the probability of rainfall occurrence at the observation point i, and $\tilde{P}$ the interpolated probability of rainfall given by Eq. (9).

2.4. Bias adjustment of stochastic model parameters

The bias adjustment approach is based on the assumption of spatial correlation in the differences in daily rainfall between the TRMM pixels and the (aggregated) gauges. Biases at pixels devoid of gauges can then be estimated by interpolating the biases observed at pixels that contain gauges. Interpolating the biases for each stochastic parameter to un-gauged pixels raises the same problems as interpolating the stochastic parameters within the pixels (Section 2.3). Thus, we independently interpolate the SMPs estimated from TRMMv6 at gauged pixels and the pixel-scale SMPs estimated from the gauges (and *not* the difference between them), before computing the biases at ungauged pixels as the difference between the two interpolations. The full bias adjustment procedure thus consists of the following steps:

(i) Aggregating the SMPs observed at the gauges to the resolution of TRMM pixels (Section 2.2).
(ii) Interpolating the aggregated SMPs from the gauged to the ungauged pixels (Section 2.3), labeled as $\widetilde{\text{SMP}}_{\text{pix}}$.
(iii) Interpolating the SMPs obtained for TRMMv6 at the gauged pixels to the ungauged pixels (Section 2.3), labeled as $\widetilde{\text{SMP}}_{\text{TRMM}}$.
(iv) Computing the biases $\widetilde{\text{SMP}}_{\text{TRMM}}$ at ungauged pixels by subtracting the result of step (ii) ($\widetilde{\text{SMP}}_{\text{pix}}$) to the result of step (iii) ($\widetilde{\text{SMP}}_{\text{TRMM}}$).
(v) Finally, biases are adjusted by subtracting the modeled bias $\widetilde{\text{SMP}}_{\text{TRMM}}$ from SMP_{TRMM}, the local SMPs of TRMMv6:

$$\begin{aligned} \text{SMP}_{\text{adjusted}} &= \text{SMP}_{\text{TRMM}} - \Delta\widetilde{\text{SMP}}_{\text{TRMM}} \\ &= \text{SMP}_{\text{TRMM}} - \left(\widetilde{\text{SMP}}_{\text{TRMM}} - \widetilde{\text{SMP}}_{\text{pix}} \right). \end{aligned}$$

Assuming rainfall follows the stochastic model described in Section 2.1, this procedure allows the bias adjusted distribution of rainfall to be estimated for all pixels.

2.5. Bias adjustment of time series

A useful application of the bias adjusted distribution of rainfall obtained in the previous section is its use to correct remotely sensed time series through quantile mapping. Quantile mapping is a well established technique (see [12] for a review) that, in the context of this paper, attempts to find a transformation of $X_{TRMM}^{(t)}$, the remotely sensed rainfall observation at time t, such that its new distribution equals the distribution of $X_{\text{adj}}^{(t)}$, the corresponding bias adjusted rainfall observation. The distribution of $X_{TRMM}^{(t)}$ can be readily characterized from remote sensing observations. The method presented in Section 2.2.3 provides the bias corrected distribution of rainfall (i.e the distribution of $X_{\text{adj}}^{(t)}$). The transformation can therefore be written as

$$X_{\text{adj}}^{(t)} = F_{\text{adj}}^{-1}(F_{\text{TRMM}}(X_{\text{TRMM}}^{(t)})) \tag{14}$$

where $F_{\text{adj}}^{-1}(\cdot)$ is the inverse of the bias adjusted cumulative distribution function and $F_{\text{TRMM}}(\cdot)$ is the cumulative distribution function of remotely sensed rainfall at the considered pixel. $F_{\text{TRMM}}(X^{(t)})$ can be calculated using the relevant stochastic model parameters obtained from remotely sensed rainfall by applying the law of total probabilities:

$$F_{\text{TRMM}}(X_{\text{TRMM}}^{(t)}) = (1 - P_{\text{TRMM}}) + P_{\text{TRMM}} \cdot F_{\text{TRMM,w}}(X_{\text{TRMM}}^{(t)}) \tag{15}$$

where $P_{\text{TRMM}} = P_{01,\text{TRMM}}$ if $X_{\text{TRMM}}^{(t-1)} = 0$ and $P_{\text{TRMM}} = P_{11,\text{TRMM}}$ otherwise; and where $F_{\text{TRMM,w}}(X^{(t)})$ is the cumulative distribution function of a gamma distribution with rate GR_{TRMM} and shape GS_{TRMM}. Similarly, the bias-adjusted cdf F_{adj} can be calculated using the bias-adjusted stochastic model parameters.

$$F_{\text{adj}}(X_{\text{adj}}^{(t)}) = (1 - P_{\text{adj}}) + P_{\text{adj}} \cdot F_{\text{adj,w}}(X_{\text{adj}}^{(t)}) \tag{16}$$

where $P_{\text{adj}} = P_{01,\text{adj}}$ if $X_{\text{adj}}^{(t-1)} = 0$ and $P_{\text{adj}} = P_{11,\text{adj}}$ otherwise; and where $F_{\text{adj,w}}(Y^{(t)})$ is the cumulative distribution function of a gamma distribution with rate GR_{adj} and shape GS_{adj}. We define the inverse of $F_{\text{adj}}(\cdot)$ as

$$F_{\text{adj}}^{-1}(Y^{(t)}) = \begin{cases} 0 & \text{if } Y^{(t)} \leqslant 1 - P_{\text{adj}} \\ F_{\text{adj,w}}^{-1}(Y^{(t)}) & \text{otherwise} \end{cases} \tag{17}$$

Note that $F_{\text{TRMM}}(\cdot)$ has a discontinuity at zero. Therefore, its image does not span all possible probabilities between zero and one (i.e. values below P_{TRMM} are excluded from the image). When applying quantile mapping (Eq. (14)) part of the rainfall range is therefore censored. For example if $F_{\text{adj}}(0) < 1 - P_{\text{TRMM}}$, all values of $X_{\text{TRMM}}^{(t)}$ will be mapped to positive rainfall.[1] In other words, a dry data point in TRMM is always matched to the *largest* rainfall value $X_{\text{adj}}^{(t)}$ that occurs with the probability $F_{\text{TRMM}}(0)$ in our model. Of course, any rainfall prediction below this cutoff would be just as reasonable. To avoid artificial overestimation of rainfall occurrence, we therefore match a dry TRMM data point to a random sample from the conditional distribution $F_{\text{adj}}(x|x \leqslant X_{\text{adj}}^{(t)})$, given by

$$F_{\text{adj}}(x|x \leqslant X_{\text{adj}}^{(t)}) = \begin{cases} \frac{F_{\text{adj}}(x)}{F_{\text{adj}}(X_{\text{adj}}^{(t)})} & \text{if } x \in [0, X_{\text{adj}}^{(t)}] \\ 1 & \text{if } x > X_{\text{adj}}^{(t)}. \end{cases} \tag{18}$$

This correction ensures that we preserve the actual rainfall distribution (including rainfall occurrence) for large samples.

To summarize, we first determine which stochastic model parameters to use according to the season of $X_{TRMM}^{(t)}$ (Monsoon vs. dry season) and the rainfall occurrence status at $X_{TRMM}^{(t-1)}$ (wet vs. dry). Then,

[1] One particular concern is artificial oscillation of rainfall occurrence during dry periods, when $P_{adj,01} < P_{\text{TRMM}} < P_{adj,11}$ (or $P_{adj,11} < P_{\text{TRMM}} < P_{adj,01}$).

- if $X^{(t)}_{TRMM} > 0$, we apply Eq. (15) to get the probability of $X^{(t)}_{TRMM}$, on which we finally apply Eq. (17) to get the corresponding quantile in the adjusted rainfall distribution.
- if $X^{(t)}_{TRMM} = 0$ we have $F_{\mathrm{TRMM}}(X^{(t)}_{\mathrm{TRMM}}) = P_{\mathrm{TRMM}}$ and are confronted to the discontinuity problem mentioned above. The case where $F^{-1}_{\mathrm{adj}}(P_{\mathrm{TRMM}}) = 0$ results in a dry day and $X^{(t)}_{\mathrm{adj}} = 0$. If $F^{-1}_{\mathrm{adj}}(P_{\mathrm{TRMM}}) > 0$, $X^{(t)}_{\mathrm{adj}}$ is stochastically determined as a random draw from the distribution, which cdf is described in Eq. (18). This is equivalent to the practically more convenient option of a random draw from the distribution in Eq. (16) with rejection of samples above $F^{-1}_{\mathrm{adj}}(P_{\mathrm{TRMM}})$.

3. Methods

The methods section describes the metrics used to evaluate the bias adjustment process of stochastic model parameters described in Section 2.4, and a Monte Carlo analysis in which the performance of the process was tested on synthetic data (Section 3.1). It then outlines the application of the technique to rainfall data in Nepal (Section 3.2). As part of this application we characterize the bias in TRMM observations (Section 3.2.3), and perform a jack-knife cross validation [25] to assess the performance of the bias-adjustment technique (Section 3.2.5). Finally, an example of the application of the adjusted stochastic model parameters to correct TRMM time series is given in Section 3.2.6. The stochastic model, bias adjustment methods and time series correction procedure were compiled in an R script [26] and are provided as supplementary material.

3.1. Monte Carlo analysis

To evaluate the performance of the bias adjustment we focus on the mean absolute errors (MAE) in annual rainfall. The MAE avoids outlier compensation effects, whereby overestimation at one gauge may cancel out the underestimation at another (leading to underestimation of the true error). The MAE of annual rainfall provides a scalar performance metric that combines errors in the occurrence, intensity and seasonality of rainfall and is easily understood in physical terms. We also compute MAEs for the variance and occurrence probability of daily rainfall.

We run a Monte Carlo analysis using synthetic data to evaluate the properties of our bias adjustment technique and its sensitivity to a range of characteristics of the gauge network and TRMM observations (presented in Table 3).

We apply the following procedure to generate a synthetic rainfall surface, TRMM data and gauge observations that are representative of our case study site (Nepal):

Table 3
Experimental variables, their default value and range considered in the Monte Carlo experiments. fAWN_{local} and fAWN_{obs} represent the standard deviation of local rainfall variations and observation errors on gauges respectively; N and z_{max} represent the size and upper altitude limit of the gauge network; fBIAS_{mean} and fBIAS_{range} the multiplication factors respectively applied on the mean amplitude and spatial auto-correlation range of the TRMM biases observed in Nepal.

Variable	Default value	Experimental range
fAWN_{local}	0	0–0.2
N	50	10–1000
z_{max}	8848	1000–8848
fAWN_{obs}	0	0–0.3
fBIAS_{mean}	1	0.5–5
fBIAS_{range}	1	0.01–2

1. The SMP values observed at Nepalese gauges are interpolated by ordinary kriging onto a 0.05° grid, which is generated from a high resolution digital elevation model of Nepal [27].
2. Synthetic SMP surfaces are created by adding white noise (with standard deviation fAWN_{local}) to each point of the grid. This additive noise represents inaccuracies associated with the interpolation and local rainfall variations that are not captured by the gauge network.
3. N grid points are randomly selected as 'rain gauge' locations. We control bias in the selection of gauge locations by specifying an elevation threshold z_{max}, and forcing all gauges to be located below this threshold.
4. Random observation errors are simulated by adding white noise with standard deviation fAWN_{obs} to the SMPs at the synthetic gauges.
5. Synthetic TRMM data are generated by spatially aggregating (Section 2.2) the synthetic SMP surfaces at the TRMM resolution of 0.25° and adding a spatially correlated random bias. The mean value and spatial correlation range of the bias are prescribed as multiples of the corresponding values observed in Nepal with multiplication factors fBIAS_{mean} and fBIAS_{range}.
6. For each of the 'real', bias-corrected and the two control procedures (interpolation of gauges only, or direct use of TRMM observations only), we also generate a surface of the expected annual rainfall, which is used as a basis for computing MAE and evaluating the bias correction technique.

We generate approximately 80 realizations of potential rainfall surfaces by varying each of the parameters in Table 3 while maintaining others at the default values listed in Table 3. We assess the MAE on the annual rainfall in each case. For each set of numerical experiments, we repeat the Monte Carlo process until the computed MAE becomes insensitive to the addition of further iterations (i.e. changes by less than 1%). The Monte Carlo estimate of the mean absolute error on yearly rainfall ($\mathrm{MAE}_{\mathrm{MC}}$) is estimated for the three regionalization procedures: our bias adjustment method, unadjusted (synthetic) TRMM and interpolated (synthetic) gauges. In order to compare the robustness of each procedure to changes in the uncertainty sources in Table 3, we normalized all $\mathrm{MAE}_{\mathrm{MC}}$ values by the mean absolute error obtained with the default parameter values (Table 3). This analysis compares the robustness of the procedures to uncertainty in the input data, but does not evaluate the absolute quality of the rainfall predictions obtained by each method.

3.2. Nepal case study

3.2.1. Study area

We used our proposed bias adjustment technique to correct TRMMv6 using rain gauge data in Nepal. Nepal lies on an escarpment bounded by the Gangetic Plain to the south and the Tibetan Plateau to the north. Its large altitudinal range spans diverse physiographic regions, from tropical lowlands to high Himalayan mountains that contain the headwaters of Asia's major river systems and thus water supply for close to 1.4 billion people [28]. This diversity is reflected in the annual rainfall observed at local gauges, which varies from 200 mm y^{-1} in the Trans-Himalayan semi-arid Mustang region, to 4000 mm y^{-1} 100 km further south near the city of Pokhara, upwind of the Annapurna Range (Fig. 1). We estimated the average annual rainfall of Nepal as 1750 mm y^{-1} via Theissen polygon weighting of gauge observations. Most precipitation occurs during the Asian summer monsoon (June to September), when the Himalayan range intercepts strong easterly winds carrying moist air from the Bay of Bengal [29]. The precipitation declines towards the west, reflecting the monsoon circulation. Orography and rain

shadows affect rainfall in the high Himalayas and the Tibetan plateau, causing rainfall to also decline towards the north [2]. These regional rainfall patterns reverse in winter (December–February), when westerly weather systems generate snowfall preferentially in the high mountains in Western Nepal. Fig. 1 shows the spatial pattern in annual rainfall for 2010 as measured by the TRMM 3B43 (v6) monthly rainfall product aggregated at the annual scale. At smaller scales, orographic effects are significant and affect both the spatial and temporal distribution of rainfall. Daytime rainfall is abundant on ridges, while rain occurs at night, and in smaller volumes, in the valleys [2].

There have been several evaluations of TRMM rainfall predictions in Nepal. TRMMv6 reliably detects monthly rainfall patterns, large-scale rainfall patterns and heavy rainfall events in the Himalayas [29–32]. At daily time scales, however, TRMMv6 consistently underestimated rainfall volume along the Himalayan range in Nepal [5,9], while overestimating it on the Tibetan Plateau [10]. A major revision of TRMM 3B42 (TRMMv7) was released in late 2012. In this revision, satellite observations are adjusted using a much larger density of rainfall gauges [33]. As discussed in the introduction, TRMMv6 in Nepal provides us with a barely-corrected satellite rainfall data product, while TRMM v7 provides a comparison with a more traditional method of bias correction, allowing us to benchmark our process against a state-of-the-art bias-adjusted product. We therefore applied the bias correction techniques to TRMMv6 data, treating TRMMv7 as a validation dataset for comparison.

3.2.2. Data sources and pre-processing

Gauge data from 192 rainfall stations for the 1969–1995 period are available from the "Hindu-Kush Himalayan Flow Regimes from International Experimental and Network Data" (HKH-FRIEND) projects Regional Hydrological Data Centre [34]. We obtained additional data from 47 gauges covering a more recent period (1998–2010) from the Department of Hydrology and Meteorology of Nepal [35]. These gauges are a subset of the 280 gauges used to generate the gridded GPCC dataset on which NASA calibrates TRMMv7.

We remove all years that were missing more than 10 days of data and use double mass plots to remove gauges with inhomogeneous data. Different datasets collected at identical locations are merged, generating a final dataset of 114 gauges, with data spans of at least 10 years. We anticipate that considerable observation error remains in this dataset, due to (at least) the diverse range of technologies and data records used at individual gauges. Fig. 1 shows the gauge locations. Gauges are scarce at elevations above 2000 masl and in the mountainous regions of northern Nepal (Fig. 1).

Remote sensing precipitation data are obtained from NASA's TRMM 3B42 v6 and v7 research products [36], and aggregated to provide daily rainfall estimates between 1998 and 2010. The daily timescale exceeds the characteristic duration of single rainfall events [29], allowing us to neglect the internal temporal structure of rainfall events.

We test for stationarity of the rainfall fields in the subset of gauges that spanned the whole 1969–2010 period by estimating the value of each SMP over a moving window of 4 years: about 160 rain events. We regress the estimates of the SMPs against time and tested the statistical significance of the regression coefficient with Student-t tests. For gauges where a statistically significant trend was identified ($p < 0.01$), we evaluated its impact on the prediction of the annual rainfall over a period of 12 years, which is the average lag between the end of the gauged record and the beginning of the TRMM datasets. For a trend in the SMP to impact the prediction of rainfall, it should generate errors in the annual rainfall prediction that are comparable to the error associated with the bias adjustment method (22% over 12 years – Section 4.4.2). The majority of gauges (75%) do not have a significant trend in yearly rainfall at the 99% confidence interval. Most (70%) of the gauges with statistically significant rainfall trends do not generate large enough changes in SMPs to affect the bias correction. SMP changes exceeding 22% arose in only 7% of the gauges, mostly on the SMPs related to conditional rainfall intensity: in these gauges, increases in the rate parameter of the gamma distribution were offset by decreases in the shape parameter, leading to little effect on the expected value of rainfall. Therefore, using SMPs computed in the 1969–2010 window provide a valid point of comparison to the SMPs computed from TRMM in the 1998–2010 period in which the satellite operated.

3.2.3. Stochastic model fit

We fit the 10-parameter stochastic model to daily precipitation at each gauge and at each TRMM pixel independently. Chi-squared tests confirm significant differences in the P_{01} and P_{11} transition probabilities, validating the use of a Markov chain model for over 90% of the gauges. Kolmogorov–Smirnov and Anderson–Darling tests indicate that a gamma distribution provides the best representation of conditional daily rainfall intensity during the wet season and is comparable to alternative distributions (exponential and log-normal) during the dry season. The calendar days representing the average start and end date of the monsoon (RnStr and RnStp) were identified by fitting a step function to the precipitation time series (Fig. 3). Once calibrated, the overall performance of the stochastic model was evaluated in terms of mean absolute error, based on its ability to reproduce yearly rainfall as well as the variance and occurrence probability of daily rainfall from the stochastic model parameters.

3.2.4. Bias adjustment performance at gauged pixels

We verify that removing the biases on the SMPs improves our estimation of the annual rainfall in pixels containing rain gauges. In these pixels, we (i) aggregate the SMPs observed at the gauges to the pixel scale, (ii) correct the SMPs of TRMMv6 using these aggregated values and (iii) evaluate the mean absolute error in estimated yearly rainfall by comparing the adjusted SMPs to rainfall observed at the gauges. The same set of gauges are used to adjust and evaluate the procedure: this first evaluation estimates the combined effects of adjusting the biases in multiple individual parameters at a point, without assessing the effect of aggregating and regionalizing the adjustment.

3.2.5. Bias adjustment performance at ungauged pixel

We regionalize the adjustments to ungauged pixels by interpolating the SMPs and their biases. We test for spatial trends by running stepwise multiple regressions of the SMP and their respective biases against (i) elevation (as a surrogate for orographic effects), (ii) latitude (as a surrogate for the east–west rainfall trend we anticipated due to Monsoonal circulation patterns) and (iii) longitude (as a surrogate for the north–south rainfall trend we anticipated due to rain-shadow effects). The coefficients resulting from the optimal combinations of covariates that minimized the Akaike Information Criterion [37] were either not significantly different from zero at the 95% confidence interval, or orders of magnitude smaller than the intercept, allowing us to use ordinary kriging to interpolate the SMPs. The biases in the SMPs were spatially auto-correlated, with ranges above 50 km for the stochastic parameters and above 25 km for their biases (Table 4).

The performance of the bias adjustment method at ungauged locations is assessed by comparing its performance to the two control methods used in the Monte Carlo analysis: (i) the interpolation of rain gauges and (ii) the direct use of unadjusted TRMMv6. The predictive performance of these three methods is assessed using

Table 4
Seasonal rainfall characteristics in Nepal and related biases. For each season, columns present the calendar day of season start, the probability of rain, the expected rain on a rainy day and the expected length of wet (Monsoon) or dry (dry season) spells. For each parameter, the expected value (E) across the gauge dataset, the standard deviation (σ) and the spatial correlation range (Rge) are given.

	Season start			P (rain)			E[rain]|wet day			E[wet spells]		
	E	(σ)	*Rge*	*E*	(σ)	*Rge*	*E*	(σ)	*Rge*	*E*	(σ)	*Rge*
	[Cal day]		[km]	[–]		[km]	[mm/day]		[km]	[day]		[km]
Monsoon												
Gauge	158	(14)	*90*	0.65	(0.17)	*125*	19.42	(6.88)	*89*	5.74	(4.55)	*170*
Bias	−1	(13)	*27*	0.09	(0.13)	*86*	−7.19	(5.12)	*54*	0.31	(4.24)	*179*
Dry Season												
Gauge	261	(10)	*56*	0.16	(0.07)	*86*	11.69	(3.13)	*150*	11.88	(5.20)	*128*
Bias	3	(13)	*49*	0.08	(0.10)	*96*	−6.98	(2.40)	*60*	−4.79	(4.51)	*124*

two independent validation datasets. (i) TRMMv7, which provides an external validation set, and (ii) jack-knife resampling of the ground gauge data, which provides an internal validation set [25]. The jack-knife procedure was applied to predict the pixel-scale rainfall characteristics for twenty percent of the 95 pixels containing rain gauges. A fraction of the remaining gauges was randomly assigned to a training set and used as input for interpolation and bias adjustment. We repeated the jack-knife resampling process approximately 50 times, again terminating the process when adding another replicate caused a change of less than 1% in the MAE. We finally computed the jack-knife estimate of the mean absolute error:

$$\mathrm{MAE}_{\mathrm{CV}} = \frac{1}{N_{\mathrm{CV}}}\sum_{j=1}^{N_{\mathrm{CV}}}\mathrm{MAE}_j \tag{19}$$

where MAE_j is the mean absolute error in cross validation round j, and N_{CV} is the total number of cross validation rounds. MAE_{CV} was estimated for annual rainfall, daily rainfall variance and daily rainfall occurrence probability. To simulate the effect of gauge network density on the performances of the three interpolation procedures, we varied the size of the training set, keeping the size of the validation set constant.

3.2.6. Application to the bias correction of time series

We finally illustrate the application of adjusted stochastic model parameters to correct time series through quantile mapping. The method was applied on the TRMM time series recorded above Darchula (1685 masl) a rain gauge location in the hilly region of western Nepal (Fig. 1 (a)). Although the gauge itself features an observation period that overlaps the TRMM time series, records from surrounding gauges were discontinued before the launch of the TRMM satellite, which illustrates the ability of the proposed method to use non-overlapping observations for bias correction. We consider the time series of daily rainfall in September 2005, a period overlapping both rainfall seasons – on average, monsoon ends on September 7th at that location. Similar to the cross validation analysis, stochastic model parameters are adjusted based on information from the neighboring gauges (i.e. excluding Darchula – the verification gauge). TRMM time series are corrected using the adjusted stochastic model parameters as described in Section 2.5. The ability of the corrected time series to reproduce the gauged daily rainfall is then assessed and compared to the performance of raw TRMM time series. Finally, for comparative purposes, we also compute TRMM time series corrected by scaling the monthly mean to match the (inverse distance weighted) mean September rainfall observed at surrounding gauges. The latter procedure is very similar to the bias correction operated by NASA on TRMMv6.

4. Results and discussion

4.1. Monte Carlo robustness analyses

Results from the Monte Carlo analysis are presented in Fig. 2, showing the results for the four numerical experiments outlined in Section 3.1. The outcome of the four experiments was similar: in all cases, combining the ground and satellite data to estimate "true" rainfall resulted in a product that was more robust to errors in either data source. For example, Fig. 2(a)–(c) show how the MAE in annual rainfall estimates responds to different kinds of error sources that impact uncertainty in the gauge data. Fig. 2(a) illustrates the effect of elevation bias in the gauge locations, Fig. 2(b) shows the effects of observation error at the gauges and Fig. 2(c) shows the effects of local rainfall heterogeneities. In each case, and for any given magnitude of the gauge based errors, the MAE computed from bias-adjusted, regionalized estimates with TRMM is much less (often approximately 30% less) than the MAE based on the gauges alone. Conversely, Fig. 2(d) assesses the effects of bias in TRMM measurements, and demonstrates that combining gauge data with TRMM stabilizes the MAE in the bias adjusted data even when TRMM itself is biased. Experiments in which both observation errors in gauges and biases in TRMM were present lead to similar results: the bias adjustment method increased the robustness of the predicted rainfall with respect to the most extreme uncertainty source.

The increased robustness arises due to the near independence of errors in satellite and ground-based rainfall measurements. Since there is not a systematic correlation in uncertainty between these datasets, their joint use stabilizes the bias adjustment method. The results of the Monte Carlo analysis suggest that the proposed bias adjustment procedure is robust to independent errors in the satellite and gauge based observations. This separation of compensating errors is likely to make this data-fusion approach a generic improvement on single-source estimates.

4.2. Evaluation of TRMM 3B42 v6 in Nepal

We found large bias in rainfall estimates in Nepal made using TRMMv6. Yearly rainfall was strongly underestimated by the raw TRMMv6 dataset with a mean bias of −539 mm y^{-1} over the study area and a mean absolute error of 580 mm y^{-1}. The 95% confidence interval around the mean bias was 703 mm y^{-1}, suggesting significant spatial variation in the bias, as illustrated in Fig. 4. TRMMv6 captures large scale rainfall gradients, but misses variations around prominent topographic features. For example, in leeward regions like Mustang TRMM over-estimated the gauged annual rainfall by over 100% (i.e. a relative bias above 1), while in windward regions like Pokhara TRMM underestimated the gauged annual rainfall by more than 50% (i.e. a relative bias smaller −1). These

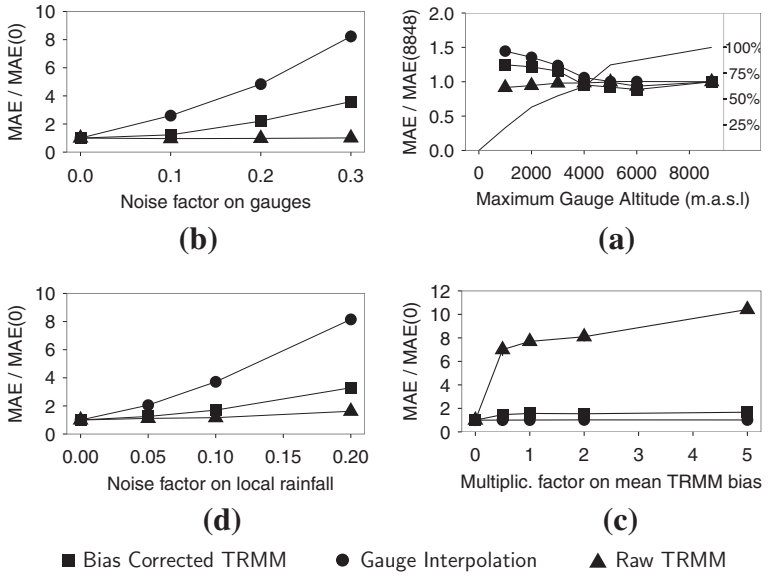

Fig. 2. Monte-Carlo simulation of the effects of uncertainty sources on the estimated annual rainfall for the bias adjustment method (squares) and the two control methods: unadjusted TRMM (triangles) and interpolation from gauges (circles). The vertical axis represents the mean absolute error on annual rainfall, normalized by its value at the default state described in Table 3. (a) Effect of the systematic selection of low altitude gauges: the x axis represents the lower altitude limit set for the randomly selected gauge locations; the graph line without point markers and secondary y axis represent the cumulative altitude distribution of the study area. (b) Effect of the variance of the random observation errors on SMPs observed at synthetic gauges. (c) Effect of the mean amplitude of the TRMM bias. (d) Effect of the variance of local random rainfall variations occurring at a spatial scale smaller than that being captured by the gauge network.

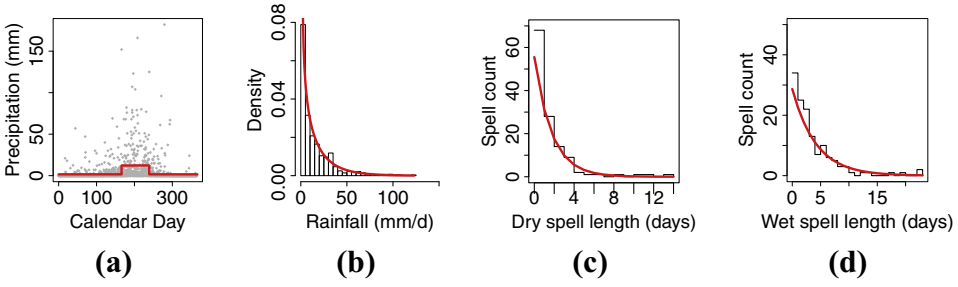

Fig. 3. Stochastic rainfall parametrization at a gauge in Western Nepal (Lat:29°28′, Long:80°32′, z = 1266 m). (a) A step function is fitted to the time series of daily rainfall to determine seasonality. Monsoon starts and ends at calendar days, when the step function is vertical. (b) A two-parameter gamma distribution is fitted on daily rainfall intensity for each season. The fit on Monsoon rainfall is represented in the figure. (c) The distribution of dry spells (here during the dry season) matches a geometric distribution with probability $P_{01}^{(d)}$. (d) The distribution of wet spells (here during the Monsoon) matches a geometric distribution with probability $P_{11}^{(w)}$.

observations are consistent with previous observations that TRMMv6 fails to reproduce orographic impacts on rainfall [4]. The observed clustering of biases around prominent topographic features leads to spatial heterogeneity in the biases, but also spatial autocorrelation, facilitating the use of kriging techniques for interpolation.

The mean, standard deviation and spatial range values for each of the stochastic rainfall characteristics described in Appendix A and calculated from the fitted SMPs are shown in Table 4. As shown, TRMMv6 reproduced the duration of the monsoon well: it occurred, on average, between June 7th and September 18th. The beginning and end dates of the monsoon period each had a standard deviation of approximately two weeks across the region. During the monsoon, 65% of the days were rainy, with average wet spells of 6 days. Only 16% of days were rainy in the dry season, with average dry spells of 12 days. These characteristics were also reproduced by TRMMv6 with a slight overestimation of daily rainfall probabilities. Conditional rainfall intensity was severely underestimated by TRMMv6 which found the intensity to be approximately 50% smaller than that reported by the gauge network. In contrast, [13] found that TRMMv6 under-estimated daily rainfall probabilities and overestimated the rainfall intensity. We attribute the differences between the findings of these studies to a different choice of evaluation metric: rather than evaluating the TRMMv6 product with respect to point gauge data, [13] compared TRMMv6 to interpolated daily precipitation measurements.

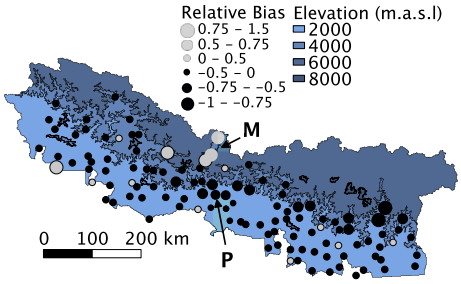

Fig. 4. Spatial repartition of the TRMM bias on yearly rainfall. The relative bias is calculated by normalizing the observed bias by the yearly rainfall measured at the gauge. A relative bias of −1 means that the average yearly rainfall observed at the gauge is double the value given by the covering TRMM pixel. The large variation and different signs between Pokhara (P) and Mustang (M), two proximate regions separated by the Anapurna Range illustrates the effect of rain shadows on the bias.

As discussed in Section 4.4.2, errors associated with spatial interpolation of rainfall gauges exceed the error sources in TRMMv6 in regions with low gauge densities. Because of such embedded interpolation errors, the evaluation of TRMMv6 against gridded precipitation stemming from interpolated gauge data is problematic.

4.3. Stochastic modeling of Nepalese rainfall

Applying the stochastic model described in Section 2.1 to rain gauge data in Nepal lead to a mean absolute error in the annual rainfall of 7.8 mm y^{-1} compared to the observed time series – 0.4% of the region's average annual rainfall of 1754 mm y^{-1}. Evaluating the stochastic model for each TRMM pixel as illustrated for one gauge in Fig. 3 lead to a mean absolute error of the same order. These results suggest that despite the complexity of Himalayan precipitation processes the local daily rainfall was well described by a simple seasonal parametric model.

4.4. Performance of the bias adjustment method in Nepal

4.4.1. Performance at gauged pixels

Adjusting the SMPs at TRMMv6 pixels that contain gauges (Section 3.2.4) reduced the mean error in annual rainfall to −9 mm y^{-1} (90% CI: 30 mm y^{-1}), effectively eliminating it. The mean *absolute* error between gauges and corrected TRMMv6 pixels was reduced by a factor of 45%, from 580 mm y^{-1} to 319 mm y^{-1}. The fact that so much error remains in the MAE indicates significant outlier compensation effects. That is, the biases are eliminated on average, but remain locally important.

4.4.2. Annual rainfall at ungauged pixels

Fig. 5 shows the results of the cross validation procedure described in Section 3.2.5, which illustrates the ability of the bias adjustment method to reproduce yearly rainfall at ungauged locations. Comparing raw TRMMv6 and TRMMv7 to gauges results in MAEs of 580 mm y^{-1} and 404 mm y^{-1} respectively. These values compare to a MAE of 443 mm y^{-1} obtained when interpolating SMPs from all available gauges. Thus, interpolating the existing gauge network in Nepal outperforms TRMMv6 in the estimation of local annual rainfall, but is surpassed by TRMMv7. The MAE related to gauge interpolation increases steadily with decreasing gauge network density, and exceeds that of the unadjusted TRMMv6 for densities below 2 gauges per 10,000 km^2; that is, an average distance between gauges of about 70 km. Using all the gauges in the training set (i.e. 80% of the total number of gauges) to adjust the bias on TRMMv6 reduced the mean absolute error in annual rainfall to 391 mm y^{-1}. This represents 22% of the region's average gauged rainfall of 1753 mm y^{-1} estimated through Thiessen polygons (Section 3.2.1). When considering the perhaps more accurate measure of average rainfall of 1233 mm y^{-1} obtained by adjusting TRMMv6 over the whole study area, the relative error increases to 31%. This includes the effect of errors related to aggregation and spatial interpolation to ungauged TRMMv6 pixels.

4.4.3. Decreasing returns to network density

The error curve for the bias adjustment on annual rainfall is shown in Fig. 5(a). This curve flattens and asymptotes to the error curve for the TRMMv7 data when all available gauges are used to correct TRMMv6. This is consistent with the large number of gauges used by TRMMv7 to adjust the remote sensing rainfall estimates. The flattening of the error curve leads to two noteworthy implications. (i) The incremental benefit of adding gauges to the network to adjust TRMMv6 decreases with increasing network density. The curvature appears to be highest at a density of about 2.5 gauges per 10,000 km^2, where the error is decreased to 458 mm y^{-1}, that is 36% of the TRMM-adjusted average rainfall using only 25% of the available gauges. Thus, a relatively sparse network of gauges, integrated in a bias adjustment procedure based on 10 parameters, efficiently corrects TRMMv6 and generates performance levels comparable to TRMMv7. (ii) The hypothetical availability of a dense gauge network e.g. observed data for every TRMM pixel to adjust TRMMv6 would result in a non-zero asymptotic error. Indeed, TRMMv7, which is calibrated on 280 gauges, does not outperform a bias adjusted TRMMv6 that uses only 91 gauges. The asymptotic error of 319 mm y^{-1} was estimated using the complete set of available gauges as training and validation sets simultaneously, overriding the aggregation and interpolation steps of the procedure. This residual error is related to omission of local rainfall variations by the coarse resolution of the TRMM satellite and spacing of the Nepalese gauges.

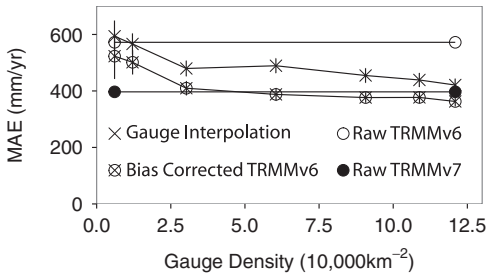

(a) Annual Rainfall

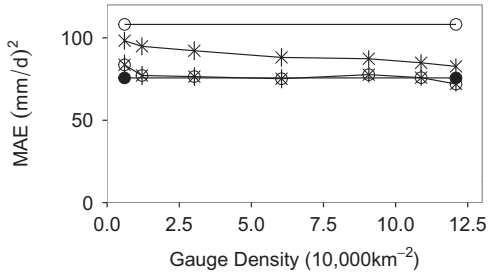

(b) Rainfall Variance

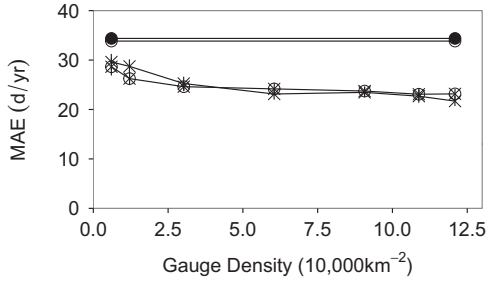

(c) Rainfall Occurence

Fig. 5. Cross validation performances of TRMMv6 (white circles), TRMMv7 (black circles), gauge interpolation (crosses) and bias adjusted TRMMv6 (crossed circles). (a) Mean absolute error on yearly rainfall prediction at ungauged location: bias adjusted TRMMv6 outperforms raw TRMMv6 and gauge interpolation and reaches the performance of TRMMv7 at gauge densities of 6 gauges per 10,000 km^2. (b) Mean absolute error on the variance of daily rainfall: Correcting TRMMv6 leads to equivalent performances than TRMMv7 and both datasets outperform TRMMv6. (c) Mean absolute error on the prediction of the average number of rainy days per year: Gauges outperform both TRMM dataset and improve the performance of bias adjusted TRMMv6.

4.4.4. Rainfall variance and occurrence probability

Fig. 5(b) and (c) show the method's performance at predicting rainfall variance and occurrence using the same cross validation approach as Section 4.4.2. For the variance of daily rainfall, the performance of TRMMv7 was reached by correcting TRMMv6 using a small subset of the gauge network. Increasing the density of gauges only slightly improved the performance of gauge-based techniques.

When considering rainfall occurrence, gauge interpolation outperformed both TRMMv6 and TRMMv7 by nearly 30%, with an average error of 21 rainy days per year when all gauges were used. This is consistent with the fact that the TRMM algorithm calibrates remote sensing data using observed monthly mean precipitations, which corrects for average rainfall intensity but fails to adjust biases on rainfall occurrence. The error curve corresponding to the bias adjustment procedure follows the curve related to gauge interpolation, showing that the proposed bias adjustment method successfully corrects rainfall occurrence. Similar to yearly rainfall, the error curve on rainfall occurrence flattens, again suggesting that the incremental benefit of adding gauges to the network to adjust TRMMv6 decreases with increasing network density.

4.4.5. TRMMv7 vs. bias-adjusted TRMMv6

Despite the availability in Nepal of high quality TRMMv7 data that successfully represents annual rainfall, the proposed approach to correct TRMMv6 finds its usefulness in its parsimony and its ability to correct hydrologically relevant rainfall statistics using a much sparser gauge network. Our approach reached the performance of TRMMv7 in the prediction of annual rainfall using a small subset (90 gauges) of the 280 gauges used in the GPCC dataset to calibrate TRMMv7. Including a stochastic model in the approach allows the daily rainfall to be corrected by adjusting 10 stationary parameters, instead of the 144 monthly means calibrated by the TRMM algorithm for each pixel over a period of 12 years. The proposed method reaches the prediction of rainfall variance and significantly improves that of rainfall occurrence in ungauged locations relative to TRMM v7, using only a subset of the gauges. Finally, we have shown that our method enables even a sparse ground gauge network to correct satellite observations to the same level of accuracy as achieved by monthly-interpolation from a dense network, suggesting that our approach will have applicability in sparsely monitored locations.

4.4.6. Bias correction of time series

Fig. 6 illustrates the use of bias-adjusted stochastic model parameters to correct TRMM time series through quantile mapping for September 2005 at Darchula (1685 masl) in Western Nepal. It is immediately clear from the figure that daily rainfall corrected through quantile mapping (circles) reproduces well the observed time series. With a mean absolute error of 8.3 mm over the considered period, the quantile mapping time series outperforms raw (dashed) and rescaled (dotted) TRMM with respective mean absolute errors of 9.5 mm and 14.9 mm – though the error of rescaled TRMM is likely dominated by gross overestimations of storms on September 15th and 24th.

However, two fundamental limitations of the method are also visible on the figure. (i) Satellites have a limited ability to detect small scale rainfall features, such as the fact that the magnitude of the September 16th storm was lower at the gauge than the pixel average. This limitation is nonetheless common to most remote sensing rainfall estimations and not specific to the proposed method. In fact, unlike mean rescaling, quantile mapping allows representing decreasing biases with rainfall intensities, which prevented the overestimation of the storm of September 24th. (ii) The proposed method addresses the discontinuity of rainfall distribution around zero by generating adjusted rainfall stochastically on days when TRMM records a dry day (8 days days in September 2005), if TRMM overestimates rainfall frequency (i.e. if $F_{adj}^{-1}(P_{TRMM}) > 0$) like in the considered case. The proposed method therefore randomly introduces occurrence errors on certain days (e.g., September 9th), while correcting them others (e.g. September 26th). However, unlike other bias correction approaches, the stochastic method improves the prediction of rainfall frequency, reducing occurrence prediction errors by about 20% at the considered gauge for time series duration of 30 days (5 to 4 errors), 1 year (78 to 57) and 5 years (506 to 401).

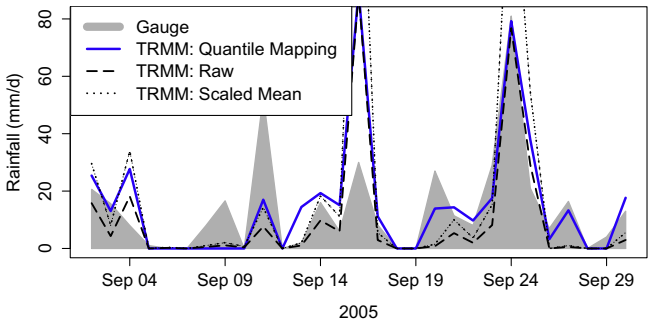

Fig. 6. Application of the bias-adjusted stochastic model parameters in a quantile mapping procedure to correct daily rainfall time series at Darchula (1683 masl) in Western Nepal. The ability of the TRMMv6 time series adjusted with the proposed method (solid) to reproduce gauged values (shaded) exceeded the performance of raw TRMMv6 (dashed) and that of rescaled TRMMv6 (dotted) – i.e. adjusted without stochastic model parameters.

5. Conclusion

This study explored the potential for bias correction techniques based on stochastic rainfall representations to provide spatially aggregated rainfall data with value for driving hydrological simulations. We have demonstrated that such methods are robust to multiple sources of error and bias in both satellite and ground-based observations of rainfall, and provide robust results for gauge densities as low as 2.5 per 10,000 km^2. We have illustrated that by separating out sources of rainfall observation bias which have different directionalities in different spatial locations, this methodology not only provides a reproduction of rainfall totals which compares to alternative bias correction approaches, such as that applied by NASA for the TRMMv7 dataset; but actually reproduces important statistical features of the rainfall time series, notably the local rainfall variance and rainfall occurrence probabilities, with greater fidelity than obtained from conventional time series bias adjustments.

While a fundamental limitation lies in the inability of satellites to observe small scale rainfall features (a limitation common to other bias adjustment approaches, as shown by the convergence of error estimates between the stochastic approach and the TRMMv7 observations), the proposed method successfully generates parametric distributions of bias-corrected rainfall using a finite number of gauges. Useful application of these results include their use as inputs to frequency domain hydrological models, the stochastic generation of synthetic rainfall or the correction of remotely sensed time series through quantile mapping.

Thus, the stochastic procedure effectively combines satellite data with sparse rain gauges, providing a robust technique for estimating rainfall properties in minimally-gauged regions, and offering insight into the minimal rainfall gauge network that could be reliably used to understand the spatio-temporal variations in precipitation in mountainous regions.

Acknowledgments

The authors thank Michèle Müller for her invaluable assistance in data analysis and coding, as well as Slav Hermanowicz and anonymous reviewers for their helpful review and comments. Data have been graciously provided by the NASA Tropical Rainfall Measurement Mission, the Department of Hydrology and Meteorology of Nepal and the HKH-FRIEND project. The Fulbright Science and Technology Fellowship and the National Science Foundation NSF EAR-1013339 are gratefully acknowledged for funding.

Appendix A. From stochastic model parameters to evaluation metrics

The output of our stochastic model are the 10 parameters described in Table 2. Combining these parameters, one can obtain seasonal metrics such as the unconditional expectation and variance of daily rainfall $(\mathsf{E}\left[X^{(i)}\right], \mathsf{Var}\left(X^{(i)}\right))$ the expected length of wet and dry spells $(L_w^{(i)}, L_d^{(i)})$ and the probability of rainfall occurring on any given day $(P^{(i)})$. These relationships are listed in Eqs. (A.1)–(A.5):

$$L_w^{(i)} = \frac{1}{1 - P_{11}^{(i)}} \tag{A.1}$$

$$L_d^{(i)} = \frac{1}{P_{01}^{(i)}} \tag{A.2}$$

$$P^{(i)} = \frac{P_{01}^{i}}{1 + P_{01}^{(i)} - P_{11}^{(i)}} \tag{A.3}$$

$$\mathsf{E}\left[X^{(i)}\right] = P^{(i)} \frac{\mathsf{GS}}{\mathsf{GR}} \tag{A.4}$$

$$\mathsf{Var}\left(X^{(i)}\right) = P^{(i)} \frac{\mathsf{GS}}{\mathsf{GR}^2} + P^{(i)}(1 - P^{(i)}) \frac{\mathsf{GS}}{\mathsf{GR}} \tag{A.5}$$

where the subscript i indicates either the wet (w) or dry (d) season. By weighing seasonal metrics by the duration of the corresponding season we get the annual metrics ($L_w, P, \mathsf{E}[X]$ and $\mathsf{Var}(X)$):

$$P = L_{\mathsf{Rn}} P^{(w)} + (1 - L_{\mathsf{Rn}}) P^{(d)} \tag{A.6}$$

$$L_w = \left(1 - \frac{L_{\mathsf{Rn}} P^{(w)} P_{11}^{(w)} + (1 - L_{\mathsf{Rn}}) P^{(d)} P_{11}^{(d)}}{P}\right)^{-1} \tag{A.7}$$

$$\mathsf{E}[X] = L_{\mathsf{Rn}} P^{(w)} \frac{\mathsf{GS}^{(w)}}{\mathsf{GR}^{(w)}} + (1 - L_{\mathsf{Rn}}) P^{(d)} \frac{\mathsf{GS}^{(d)}}{\mathsf{GR}^{(d)}} \tag{A.8}$$

$$\begin{aligned}\mathsf{Var}(X) = {} & L_{\mathsf{Rn}} \left(\frac{\mathsf{GS}^{(w)}}{\mathsf{GR}^{(w)}}\right)^2 + (1 - L_{\mathsf{Rn}}) \left(\frac{\mathsf{GS}^{(d)}}{\mathsf{GR}^{(d)}}\right)^2 \\ & - \left(L_{\mathsf{Rn}} \frac{\mathsf{GS}^{(w)}}{\mathsf{GR}^{(w)}} + (1 - L_{\mathsf{Rn}}) \frac{\mathsf{GS}^{(d)}}{\mathsf{GR}^{(d)}}\right)^2 + L_{\mathsf{Rn}} \frac{\mathsf{GS}^{(w)}}{\mathsf{GR}_{(w)}^2} + (1 \\ & - L_{\mathsf{Rn}}) \frac{\mathsf{GS}^{(d)}}{\mathsf{GR}_{(d)}^2}\end{aligned} \tag{A.9}$$

with $L_{\mathsf{Rn}} = (\mathsf{RnStp} - \mathsf{RnStr})/365$, the fraction of the year occupied by the rainy season. Finally, yearly rainfall and the average number of rainy days per year can easily be obtained by multiplying $\mathsf{E}[X]$ and P by 365 respectively.

Appendix B. Aggregation of rainfall occurrence probabilities

A pixel is in a rainy state on a given day if it rains at *any* of its gauges during that day, which precludes an area weighting approach from being applied to aggregate rain occurrence parameters. Indeed, let a pixel contain two gauges with equal weights and rainfall probabilities of 0.1 and 1 respectively: because it rains every day at one of the gauges, rainfall probability at the pixel level will be 1, which is not the average of the probabilities at the gauges.

Assuming a pixel contains N_p gauges with rainfall probabilities P_i , the following bounds apply:

$$\max P_i \leqslant P_{\mathsf{pix}} \leqslant \min\left\{\sum_{i=1}^{N_p} P_i, 1\right\} \tag{B.1}$$

P_{pix} reaches the lower bound if the correlation between rain occurrence is positive and maximal, i.e. a dry day at the gauge with highest P always corresponds to a dry day for the pixel. The higher bond is reached if the correlation is negative with a maximal absolute value, i.e. it almost always rains on at least one of the gauges.

In order to satisfy the two degrees of freedom offered by the two Markov transition probabilities (P_{01} and P_{11}) considered as SMPs, a the aggregation of a second metric (other than P_i) must be considered. The pixel aggregated value of $P_{\mathsf{pix}} \cdot P_{11,\mathsf{pix}}$, the ratio of a wet-to-wet transitions, is bounded by

$$\max\left(P_i \cdot P_{11,i}\right) \leqslant P_{\mathsf{pix}} \cdot P_{11,\mathsf{pix}}$$

because such a transition occurring at a gauge is a *sufficient* condition for it to be aggregated at the pixel level. Similarly,$P_{\mathsf{pix}} \cdot P_{10,\mathsf{pix}}$, the ratio of a wet-to-dry transitions is bounded by

$$\sum_{i=1}^{N_p} P_i \cdot P_{10,i} \geqslant P_{\mathsf{pix}} \cdot P_{10,\mathsf{pix}}$$

because such a transition occurring at the gauge level is a *necessary* condition for it to be aggregated at the pixel level. Finally, both transition ratios are bounded by the maximum probability of rainfall according to inequality (B.1). Therefore, with $P_{11} = 1 - P_{10}$, the bounds on $P_{11,\mathsf{pix}}$ can be written as:

$$\begin{aligned}\max\left\{\frac{\max\left(P_i \cdot P_{11,i}\right)}{P_{\mathsf{pix}}}; 1 - \frac{\sum_{i=1}^{N_p} P_i \cdot (1 - P_{11,i})}{P_{\mathsf{pix}}}\right\} \leqslant P_{11,\mathsf{pix}} \\ \leqslant \min\left\{\frac{\sum_{i=1}^{N_p} P_i}{P_{\mathsf{pix}}}, 1\right\}\end{aligned} \tag{B.2}$$

Within these bounds, rainfall probability and the ratio of a wet-to-wet transitions increase with the pixel size and the number of gauges within the pixel. The actual value of these metrics depends on the spatial auto-correlation of rainfall occurrences within the pixels. If rain occurrence is highly spatially auto-correlated, which is likely in pixels smaller than the spatial scale of typical rain events, we can approximate:

$$P_{\mathsf{pix}} \approx \max P_i \tag{B.3}$$

$$P_{11,\mathsf{pix}} \approx \max\left\{\frac{\max(P_i \cdot P_{11,i})}{P_{\mathsf{pix}}}; 1 - \frac{\sum_{i=1}^{N_p} P_i \cdot (1 - P_{11,i})}{P_{\mathsf{pix}}}\right\} \tag{B.4}$$

With spatial autocorrelation ranges of approximately 3 (dry season) to 4 (wet season) times the pixel size of 27.7 km considered in Nepal (Table 4), a Monte Carlo analysis showed that these approximations lead to an average underestimation of less then 2% for both metrics for up to five gauges per pixel. This error increases with the number of gauges and decreases with the range of spatial autocorrelation.

Appendix C. Aggregation of conditional rainfall depth distribution

Consider a square pixel of side d with N_p gauges, each covering a Thiessen Polygon of size a_i, where the weights a_i are normalized such that $\sum_{i=1}^{N_p} a_i = 1$. For each gauge i, we have access to daily precipitation data X_i, as well as the statistics $\mathrm{E}[X_i|\mathrm{wet}]$ and $\mathrm{Var}(X_i|\mathrm{wet})$, measuring the mean and the variance of local rainfall on a rainy day respectively. Assuming that the precipitation depth on wet days follows a gamma distribution, these statistics can be straightforwardly related to the shape (GS) and rate (GR) of that distribution:

$$\mathrm{E}[X|\mathrm{wet}] = \frac{GS}{GR}$$

$$\mathrm{Var}(X|\mathrm{wet}) = \frac{GS}{GR^2}$$

We wish to estimate $\mathrm{E}[X_{\mathrm{pix}}|\mathrm{wet}]$ and $\mathrm{Var}(X_{\mathrm{pix}}|\mathrm{wet})$, the mean and variance of the areal rainfall on wet days aggregated at the pixel level, which will lead us to GS_{pix} and GR_{pix} the aggregated parameters of our stochastic model.

As a first step, we determine the local rainfall at a random point of the pixel X_{pt} according a two-step data generating process as follows:

(i) At the outset, before any measurements are made, a point of the pixel is chosen uniformly at random. As a result, the area weights a_i measure the probability that this point is located in Thiessen Polygon i.
(ii) Subsequently, we assume that local rainfall across the entire Thiessen Polygon is constant and measured by gauge i.

As a result, we can determine the expected unconditional rainfall at a random point of the pixel using the law of iterated expectation,

$$\mathrm{E}[X_{\mathrm{pt}}] = \mathrm{E}[\mathrm{E}[X_{\mathrm{pt}}|i]] = \sum_{i=1}^{N_p} a_i \mathrm{E}[X_i]$$

Here, $\mathrm{E}[X_{\mathrm{pt}}|i]$ denotes the expected rainfall conditional on the random point being in Polygon i, in which case X_{pt} is equal to X_i by assumption. Knowing that the mean value over the pixel area of all possible realizations of the point process X_{pt} results in an areal rainfall process with an identical expectation [22] (i.e. $\mathrm{E}[X_{\mathrm{pix}}] = \mathrm{E}[X_{\mathrm{pt}}]$), we can calculate the mean areal rainfall on a rainy day by applying the law of iterated expectations both at the pixel level and for each individual gauge,

$$\mathrm{E}[X_{\mathrm{pix}}|\mathrm{wet}] = \frac{1}{P_{\mathrm{pix}}} \cdot \sum_{i=1}^{N_p} a_i P_i \mathrm{E}[X_i|\mathrm{wet}] \tag{C.1}$$

with P_i and P_{pix} the probability or rainfall at the gauge i and at the pixel level respectively and represent the expectations of the binomial stochastic processes defining rainfall occurrence at these points.

For the local variance, the same data generating process implies, by the law of total variance,

$$\begin{aligned}\mathrm{Var}(X_{\mathrm{pt}}) &= \mathrm{E}[\mathrm{Var}(X_{\mathrm{pt}}|i)] + \mathrm{Var}(\mathrm{E}[X_{\mathrm{pt}}|i]) \\ &= \mathrm{E}[\mathrm{Var}(X_i)] + \mathrm{E}\left[\mathrm{E}[X_i]^2\right] - \mathrm{E}[\mathrm{E}[X_i]]^2 \\ &= \sum_{i=1}^{N_p} a_i \mathrm{Var}(X_i) + \sum_{i=1}^{N_p} a_i \mathrm{E}[X_i]^2 - \left(\sum_{i=1}^{N_p} a_i \mathrm{E}[X_i]\right)^2\end{aligned}$$

Again, we condition on the polygon i and assume that precipitation is homogenous within each Thiessen polygon (i.e. $X_{\mathrm{pt}} = X_i$). From Eq. (C.1), we get:

$$\mathrm{Var}(X_{\mathrm{pt}}) = \sum_{i=1}^{N_p} a_i \mathrm{Var}(X_i) + \sum_{i=1}^{N_p} a_i \mathrm{E}[X_i]^2 - P_{\mathrm{pix}}^2 \mathrm{E}[X_{\mathrm{pix}}|\mathrm{wet}]^2 \tag{C.2}$$

In the next step, we condition on rainfall probability, applying the law of total variance and taking rainfall occurrence as a binomial random variable:

$$\begin{aligned}\mathrm{Var}(X_i) &= \mathrm{Var}(\mathrm{E}[X_i|\mathrm{wet}]) + \mathrm{E}[\mathrm{Var}(X_i|\mathrm{wet})] \\ &= P_i(1-P_i)\mathrm{E}[X_i|\mathrm{wet}] + P_i \mathrm{Var}(X_i|\mathrm{wet})\end{aligned} \tag{C.3}$$

Substituting Eq. (C.3) in Eq. (C.2) we have:

$$\begin{aligned}(1-P_{\mathrm{pix}})P_{\mathrm{pix}}\mathrm{E}[X_{\mathrm{pix}}|\mathrm{wet}] + P_{\mathrm{pix}}\mathrm{Var}(X_{\mathrm{pt}}|\mathrm{wet}) &= P_i(1-P_i)\mathrm{E}[X_i|\mathrm{wet}] \\ + P_i \mathrm{Var}(X_i|\mathrm{wet}) + \sum_{i=1}^{N_p} a_i \mathrm{E}[X_i]^2 - P_{\mathrm{pix}}^2 \mathrm{E}[X_{\mathrm{pix}}|\mathrm{wet}]^2&\end{aligned}$$

Using Eq. (C.1) to express $P_{\mathrm{pix}}\mathrm{E}[X_{\mathrm{pix}}|\mathrm{wet}]$ and rearranging, we get the expression for the point variance:

$$\begin{aligned}\mathrm{Var}(X_{\mathrm{pt}}|\mathrm{wet}) = \sum_{i=1}^{N_p} \frac{a_i P_i}{P_{\mathrm{pix}}} \left[\mathrm{Var}(X_i|\mathrm{wet}) + P_i^2 \mathrm{E}[X_i|\mathrm{wet}]^2 + (P_{\mathrm{pix}} - P_i)\mathrm{E}[X_i|\mathrm{wet}]\right] \\ - P_{\mathrm{pix}}\mathrm{E}[X_{\mathrm{pix}}|\mathrm{wet}]^2\end{aligned} \tag{C.4}$$

Finally, following Rodriguez-Iturbe and Mejía [22], we can infer the variance of area rainfall X_{pix} from that of the point rainfall process X_{pt} by correcting it with a factor

$$C(d) = \int^{\sqrt{2}d} r(v) f(v) \mathrm{d}v \leqslant 1,$$

where $r(v)$ is the spatial correlation function and $f(v)$ the distribution of distances between two points chosen at random in the pixel. In other words, $\mathrm{Var}(X_{\mathrm{pix}}) = C(d) \cdot \mathrm{Var}(X_{\mathrm{pt}})$, implying that point rainfall typically overestimates the variance of area rainfall because the area averaged intensity of local rainfall events are dampened by the absence of rain in parts of the pixels that do not fall in the current extent of the storm. It directly follows that the attenuation factor $C(d)$ is increasing in pixel size d and decreasing in spatial autocorrelation range. For TRMM pixels in Nepal, where pixel size and spatial auto-correlation are spatially homogenous, we have estimated $C(27.7\ \mathrm{km})$ at 0.75 in the monsoon and 0.86 in the dry season, using a correlogram estimated based on the spatial distribution of rainfall occurrences at gauges on 2,000 randomly drawn days. Therefore, we can express the conditional variance of areal rainfall at the pixel level as a function of the moments of conditional rainfall measured at the gauges:

$$\begin{aligned}&\mathrm{Var}(X_{\mathrm{pix}}|\mathrm{wet}) \\ &= \sum_{i=1}^{N_p} \frac{C(d) a_i P_i}{P_{\mathrm{pix}}} \left[\mathrm{Var}(X_i|\mathrm{wet}) + P_i \mathrm{E}[X_i|\mathrm{wet}]^2 + (P_{\mathrm{pix}} - P_i)\mathrm{E}[X_i|\mathrm{wet}]\right] \\ &\quad - C(d) P_{\mathrm{pix}} \mathrm{E}[X_{\mathrm{pix}}|\mathrm{wet}]^2\end{aligned}$$

Finally, using Eq. (C.1) and rearranging the terms we can write:

$$\begin{aligned}\mathrm{Var}(X_{\mathrm{pix}}|\mathrm{wet}) = \frac{C(d)}{P_{\mathrm{pix}}} \left[\sum_{i=1}^{N_p} a_i P_i \left(\mathrm{Var}(X_i|\mathrm{wet}) + P_i \mathrm{E}[X_i|\mathrm{wet}]^2 - P_i \mathrm{E}[X_i|\mathrm{wet}]\right)\right] \\ + C(d) P_{\mathrm{pix}} \left[\mathrm{E}[X_{\mathrm{pix}}|\mathrm{wet}] - \mathrm{E}[X_{\mathrm{pix}}|\mathrm{wet}]^2\right]\end{aligned} \tag{C.5}$$

In essence, in order to aggregate point rainfall distribution from gauges to areal distribution at on the pixel, we first aggregate the probability of rainfall occurrence P_{pix} and ratio of wet-to-wet transitions $P_{\mathrm{pix}} \cdot P_{11\mathrm{pix}}$ (Appendix B). We use the former to aggregate the

conditional expectation of rainfall $\mathrm{E}[X_{\mathrm{pix}}|\mathrm{wet}]$. Both parameters are then used to aggregate the conditional variance $\mathrm{Var}(X_{\mathrm{pix}}|\mathrm{wet})$. The procedure is repeated for both seasons and the four related parameters of our stochastic model (P_{11}, P_{01}, GR, GS) are calculated based on the four aggregated metrics.

For interpolation we assume that the interpolated mean and variance of conditional rainfall is a linear combination of the corresponding moments of conditional rainfall at the observation points. This allows us to apply an identical procedure as above, replacing area weights a_i with interpolation weights and setting $C(d) = 1$, as no point to areal rainfall transformation occurs.

Appendix D. Supplementary data

Supplementary data associated with this article can be found, in the online version, at http://dx.doi.org/10.1016/j.advwatres.2013.08.004.

References

[1] Yatheendradas Soni, Wagener Thorsten, Gupta Hoshin, Unkrich Carl, Goodrich David, Schaffner Mike, Stewart Anne. Understanding uncertainty in distributed flash flood forecasting for semiarid regions. Water Resour Res 2008;44(5). http://dx.doi.org/10.1029/2007WR005940.

[2] Kansakar SR, Hannah DM, Gerrard J, Rees G. Spatial pattern in the precipitation regime of Nepal. Int J Climatol 2004;24(13):1645–59. http://dx.doi.org/10.1002/joc.1098.

[3] Huffman GJ, Bolvin DT, Nelkin EJ, Wolff DB, Adler RF, Gu G, Hong Y, Bowman KP, Stocker EF. The TRMM multisatellite precipitation analysis (TMPA): quasi-global, multiyear, combined-sensor precipitation estimates at fine scales. J Hydrometeorol 2007;8(1):38–55. http://dx.doi.org/10.1175/JHM560.1.

[4] Chen Y, Ebert EE, Walsh KJE, Davidson NE. Evaluation of TRMM 3b42 precipitation estimates of tropical cyclone rainfall using PACRAIN data. J Geophys Res Atmos 2013. http://dx.doi.org/10.1002/jgrd.50250.

[5] Andermann C, Bonnet S, Gloaguen R. Evaluation of precipitation data sets along the Himalayan front. Geochem Geophys Geosyst 2011;12(7):Q07023. http://dx.doi.org/10.1029/2011GC003513.

[6] Bookhagen B, Burbank DW. Topography, relief, and TRMM-derived rainfall variations along the Himalayas. Geophys Res Lett 2006;33(8):L08405. http://dx.doi.org/10.1029/2006GL026037.

[7] Shrestha MS. Bias-adjustment of satellite-based rainfall estimates over the central Himalayas of Nepal for flood prediction. PhD thesis, Kyoto University; 2011.

[8] Ward E, Buytaert W, Peaver L, Wheater H. Evaluation of precipitation products over complex mountainous terrain: a water resources perspective. Adv Water Resour 2011;34(10):1222–31. http://dx.doi.org/10.1016/j.advwatres.2011.05.007.

[9] Islam MN, Das S, Uyeda H. Calibration of TRMM derived rainfall over Nepal during 1998–2007. Open Atmos Sci J 2010;4:12–23. http://dx.doi.org/10.2174/1874282301004010012.

[10] Yin ZY, Zhang X, Liu X, Colella M, Chen X. An assessment of the biases of satellite rainfall estimates over the Tibetan Plateau and correction methods based on topographic analysis. J Hydrometeorol 2008;9(3):301–26. http://dx.doi.org/10.1175/2007JHM903.1.

[11] Cheema MJM, Bastiaanssen WGM. Local calibration of remotely sensed rainfall from the TRMM satellite for different periods and spatial scales in the Indus Basin. Int J Remote Sens 2012;33(8):2603–27. http://dx.doi.org/10.1080/01431161.2011.617397.

[12] Gudmundsson L, Bremnes JB, Haugen JE, Engen Skaugen T. Technical note: Downscaling RCM precipitation to the station scale using quantile mapping – a comparison of methods. Hydrol Earth Syst Discuss 2012;9:6185–201. http://dx.doi.org/10.5194/hessd-9-6185-2012.

[13] Duncan J, Biggs EM. Assessing the accuracy and applied use of satellite-derived precipitation estimates over Nepal. Appl Geogr 2012;34:626–38. http://dx.doi.org/10.1016/j.apgeog.2012.04.001.

[14] Laio F, Porporato A, Ridolfi L, Rodriguez-Iturbe Ignacio. Plants in water-controlled ecosystems: active role in hydrologic processes and response to water stress. II: Probabilistic soil moisture dynamics. Adv Water Resour 2001;24(7):707–23.

[15] Botter G, Porporato A, Rodriguez-Iturbe I, Rinaldo A. Basin-scale soil moisture dynamics and the probabilistic characterization of carrier hydrologic flows: slow, leaching-prone components of the hydrologic response. Water Resour Res 2007;43(2):2417. http://dx.doi.org/10.1029/2006WR005043.

[16] Srikanthan R, McMahon TA. Stochastic generation of annual, monthly and daily climate data: a review. Hydrol Earth Syst Sci 2001;5(4):653–70. http://dx.doi.org/10.5194/hess-5-653-2001.

[17] Richardson CW. Stochastic simulation of daily precipitation, temperature, and solar radiation. Water Resour Res 1981;17(1):182–90. http://dx.doi.org/10.1029/WR017i001p00182.

[18] Jimoh OD, Webster P. The optimum order of a Markov chain model for daily rainfall in Nigeria. J Hydrol 1996;185(1):45–69. http://dx.doi.org/10.1007/s00704-008-0051-3.

[19] Wilks DS. Multisite generalization of a daily stochastic precipitation generation model. J Hydrol 1998;210(1):178–91. http://dx.doi.org/10.1016/S0022-1694(98)00186-3.

[20] Brissette FP, Khalili M, Leconte R. Efficient stochastic generation of multi-site synthetic precipitation data. J Hydrol 2007;345(3):121–33. http://dx.doi.org/10.1016/j.jhydrol.2007.06.035.

[21] Huffman GJ, Bolvin DT. Trmm and other data precipitation data set documentation. Technical report, Mesoscale Atmospheric Processes Laboratory, NASA Goddard Space Flight Center; 2013.

[22] Rodriguez-Iturbe Ignacio, Mejía José M. On the transformation of point rainfall to areal rainfall. Water Resour Res 1974;10(4):729–35. http://dx.doi.org/10.1029/WR010i004p00729.

[23] Pebesma Edzer J. Multivariable geostatistics in S: the gstat package. Comput Geosci 2004;30:683–91. http://dx.doi.org/10.1016/j.cageo.2004.03.012.

[24] Ribeiro PJ, Diggle PJ. geoR: a package for geostatistical analysis. R-NEWS, 1609-3631 2001;1(2):14–8. Available from: <http://CRAN.R-project.org/doc/Rnews/>.

[25] Shao J, Tu D. The jackknife and bootstrap. New York: Springer-Verlag; 1995.

[26] Ihaka R, Gentleman R. R: A language for data analysis and graphics. J Comput Graph Stat 1996;5(3):299–314. http://dx.doi.org/10.1080/10618600.1996.10474713.

[27] NASA and JAXA; January 2013. <http://asterweb.jpl.nasa.gov/gdem.asp>.

[28] Immerzeel WW, van Beek LPH, Bierkens MFP. Climate change will affect the Asian water towers. Science 2010;328(5984):1382–5. http://dx.doi.org/10.1126/science.1183188.

[29] Bhatt BC, Nakamura K. Characteristics of monsoon rainfall around the Himalayas revealed by TRMM precipitation radar. Mon Weather Rev 2005;133(1):149–65. http://dx.doi.org/10.1175/MWR-2846.1.

[30] Anders AM, Roe GH, Hallet B, Montgomery DR, Finnegan NJ, Putkonen J. Spatial patterns of precipitation and topography in the Himalaya. Spec Pap Geol Soc Am 2006;398:39. http://dx.doi.org/10.1130/2006.2398(03).

[31] Barros AP, Joshi M, Putkonen J, Burbank DW. A study of the 1999 monsoon rainfall in a mountainous region in central Nepal using TRMM products and rain gauge observations. Geophys Res Lett 2000;27(22):3683–6. http://dx.doi.org/10.1029/2000GL011827.

[32] Yamamoto MK, Ueno K, Nakamura K. Comparison of satellite precipitation products with rain gauge data for the Khumb region, Nepal Himalayas. J Meteorol Soc Jpn 2011;89(6):597–610. http://dx.doi.org/10.2151/jmsj.2011-601.

[33] Prakash Satya, Mahesh C, Gairola RM. Comparison of TRMM multi-satellite precipitation analysis (TMPA)-3B43 version 6 and 7 products with rain gauge data from ocean buoys. Remote Sens Lett 2013;4(7):677–85. http://dx.doi.org/10.1080/2150704X.2013.783248.

[34] HKH-FRIEND; August 2011. <http://www.hkh-friend.net.np/rhdc.html>.

[35] Department of Hydrology and Meteorology. Kathmandu; September 2011.

[36] NASA; November 2012. <http://mirador.gsfc.nasa.gov>.

[37] Venables WN, Ripley BD. Modern applied statistics with S. New York: Springer-Verlag; 2002.